Localised solid-state nanopore fabrication via controlled breakdown using on-chip electrodes

Jasper P. Fried[1,2] (✉), Jacob L. Swett[1], Binoy Paulose Nadappuram[3], Aleksandra Fedosyuk[3], Alex Gee[1], Ondrej E. Dyck[4], James R. Yates[5], Aleksandar P. Ivanov[3], Joshua B. Edel[3], and Jan A. Mol[6]

[1] Department of Materials, University of Oxford, Oxford, OX1 3PH, UK

[2] School of Chemistry, University of New South Wales, Sydney, New South Wales 2052, Australia

[3] Department of Chemistry, Imperial College London, London, W12 0BZ, UK

[4] Center for Nanophase Materials Sciences, Oak Ridge National Laboratory, Oak Ridge, TN 37830, USA

[5] Instituto de Tecnologia Química e Biológica António Xavier, Universidade Nova de Lisboa, Av. da República, Oeiras 2780-157, Portugal

[6] School of Physics and Astronomy, Queen Mary University of London, London, E1 4NS, UK

ABSTRACT

Controlled breakdown has recently emerged as a highly accessible technique to fabricate solid-state nanopores. However, in its most common form, controlled breakdown creates a single nanopore at an arbitrary location in the membrane. Here, we introduce a new strategy whereby breakdown is performed by applying the electric field between an on-chip electrode and an electrolyte solution in contact with the opposite side of the membrane. We demonstrate two advantages of this method. First, we can independently fabricate multiple nanopores at given positions in the membrane by localising the applied field to the electrode. Second, we can create nanopores that are self-aligned with complementary nanoelectrodes by applying voltages to the on-chip electrodes to locally heat the membrane during controlled breakdown. This new controlled breakdown method provides a path towards the affordable, rapid, and automatable fabrication of arrays of nanopores self-aligned with complementary on-chip nanostructures.

KEYWORDS

solid-state nanopores, dielectric breakdown, nanofabrication, single-molecule sensing, nanopore arrays

1   Introduction

Solid-state nanopore devices have received interest in recent years for applications ranging from protein analysis [1–3], to polymer data storage [4, 5], and ultra-dilute analyte detection [6–9]. These devices typically consist of a nanometre-scale hole in a synthetic material that separates two chambers of electrolyte solution. When a voltage is applied across the membrane, ions flow through the nanopore resulting in a measurable ionic current. Sensing is then typically achieved by detecting changes in the ionic current as an analyte translocates through the pore and modifies the flow of ions [10–12].

In recent years, there has been a significant interest in integrating solid-state nanopores with on-chip electrodes. In particular, electrodes embedded within, or in close proximity to a nanopore can be used to control the translocation dynamics of biomolecules [13–16] or enable dielectrophoretic concentrating of analytes at the nanopore opening [17]. Solid-state nanopores have also been integrated with field-effect sensors [18–22] and tunnelling nanogap electrodes [23–27]. Measuring the conduction through such nanoelectrodes provides an alternative readout mechanism to ionic current based detection. Integrating a nanopore with a plasmonic nanostructure can also enable/enhance optical nanopore sensing strategies [28–32].

Importantly, unlike ionic current based detection, these alternative readout mechanisms do not require individual nanopores to be fluidically isolated for the signal from each pore to be read out independently [18]. As such, these alternate sensing modalities can increase the obtainable device density thus enabling high-throughput and parallel detection for quantitative analysis. Moreover, these alternative readout mechanisms can provide sensitivity to molecular properties not possible using ionic current based detection [22, 33] and increase the detection bandwidth [18, 34].

Despite the advantages provided by integrating on-chip electrodes with solid-state nanopores, the potential of these devices is yet to be fully explored. This has been partly due to challenges associated with accurately and reliably aligning a nanopore with the on-chip nanoelectrodes [20, 35, 36]. In the past, this was often done by drilling the nanopore using a focused beam of charged particles such as those created in a transmission electron microscope (TEM). However this has several drawbacks including (i) manual alignment is needed, (ii) it is a low throughput process, (iii) it requires trained operators, and (iv) it utilises expensive equipment. Developing scalable and accessible methods to fabricate solid-state nanopores integrated with on-chip nanoelectrodes would significantly accelerate research into this field.

Address correspondence to j.fried@unsw.edu.au

In recent years, controlled breakdown (CBD) has emerged as an accessible method to create solid-state nanopores [37–39]. This technique relies on applying a large electric field across the membrane to induce breakdown and nanopore formation in the dielectric. In its most commonly used form, CBD is performed by applying the breakdown voltage to electrolyte solutions in contact with either side of the membrane. However, this method should only be used to fabricate a single nanopore since new breakdown events will result in the uncontrollable expansion of previously created pores [38, 40]. Moreover, the most common form of CBD does not allow for control of the resulting pore position [41]. To overcome this issue, several CBD techniques have been developed that enable control over the nanopore position. These have included using an atomic force microscope tip to apply the voltage [42, 43], thinning a region of the membrane prior to breakdown [44], and confining the electrolyte on one side of the membrane [45–47]. These techniques have been used to integrate nanopores with on-chip structures such as microfluidics [48] and microwells [49]. However, alignment with nanoscale features has yet to be fully demonstrated. Moreover, some of these methods require relatively expensive equipment thus reducing the main appeal of CBD. Another technique that has been demonstrated relies on illuminating a plasmonic nanostructure with a laser during CBD. This results in nanopore formation at the center of the plasmonic hotspot [50]. To date, this is the only CBD method that has been used to integrate nanopores with on-chip nanostructures. While this is a highly appealing technique, it can only be used to fabricate a single nanopore in the membrane since additional breakdown events would result in the uncontrollable expansion of previously created pores. Moreover, this method requires optical equipment and can only be used to integrate nanopores with plasmonic nanostructures thus limiting its applicability for certain applications.

Here, we report a new CBD strategy whereby breakdown is performed by applying a voltage between an on-chip electrode and an electrolyte solution in contact with the other side of the membrane. This new CBD strategy possesses two main advantages. First, by localising the applied electric field to an on-chip electrode we are able to independently fabricate multiple nanopores in the membrane and control their location. Second, by applying appropriate voltages to the on-chip electrodes to locally heat the membrane during CBD, we are able to fabricate nanopores self-aligned with complementary nanostructures. With further development, we are confident that this CBD strategy could be used to fabricate high density arrays of nanopores self-aligned with on-chip nanostructures in a rapid and affordable fashion. The development of such a technique would significantly accelerate research in this field and open up routes for the commercial development of these devices.

2 Independent fabrication of multiple nanopores

First, we will demonstrate that multiple nanopores can be independently fabricated via CBD by applying the breakdown voltage between an on-chip electrode and an electrolyte solution in contact with the other side of the membrane. A schematic of the device geometry and experimental setup used for these measurements is shown in Fig. 1(a). A false-colour scanning electron microscope (SEM) image of the electrode configuration over the suspended region of SiN_x is shown in Fig. 1(b). The devices consist of a thin SiN_x membrane suspended on 500 nm of
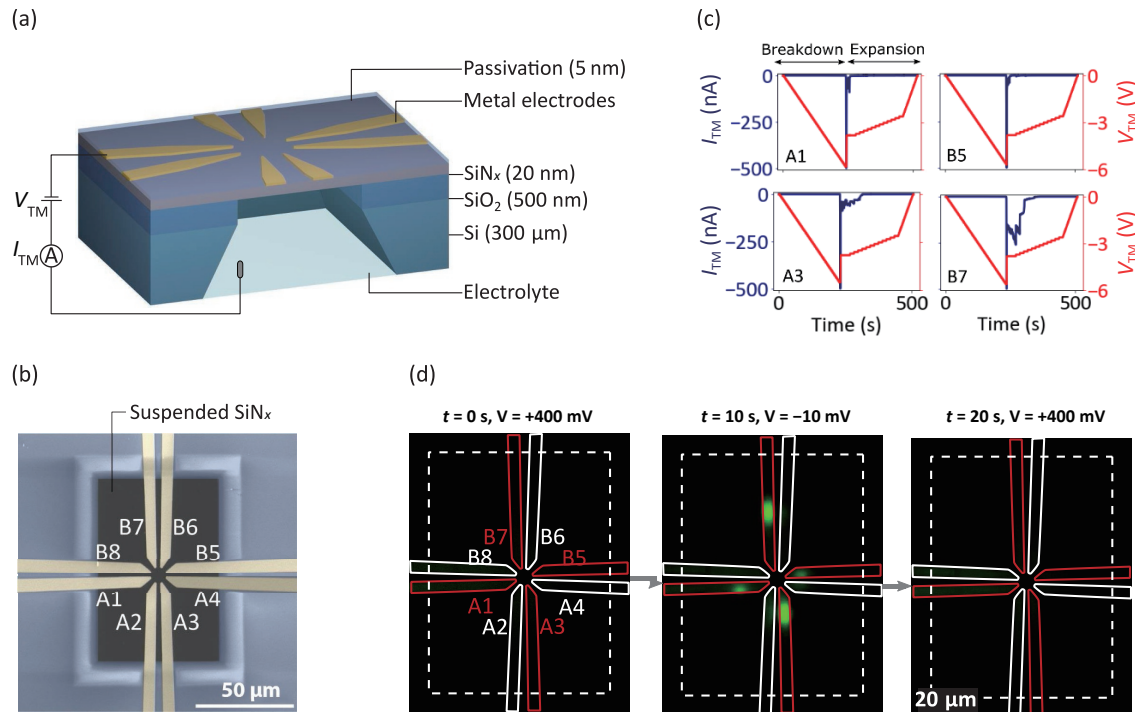

Figure 1 (a) Schematic of the device geometry and experimental setup used to independently fabricate nanopores when the breakdown voltage is applied between an on-chip electrode and an electrolyte solution. (b) False-colour scanning electron micrograph of the electrode configuration over the suspended region of SiN_x (dark grey rectangle). Electrodes are labelled A1-A4 and B5-B8 for convenience in the below discussion (the labels are not part of the device geometry). (c) CBD measurements performed on four different electrodes on the same membrane. The electrode which CBD was performed on is shown in the upper left-hand corner of each plot. The region in the leadup to breakdown, and the expansion region (to avoid soft-breakdown) is labelled in the curve for electrode A1. (d) Fluorescence micrographs of the nanopores created from the CBD measurements shown in (c). There are three micrographs showing a time series of data with a frame before (left), during (middle), and after (right) the application of a voltage that drives Ca^{2+} ions through the nanopore. The dashed white box shows the edge of the region of suspended SiN_x. The solid lines show the electrode positions with red lines for electrodes CBD were performed on and white lines for electrodes CBD were not performed on.

SiO_2 on a Si substrate. There are eight independently addressable metal (5/95/10 nm Ti/Pt/Ti) electrodes patterned on the SiN_x membrane (for convenience we have labelled these A1-A4 and B5-B8 as shown in Fig. 1(b)). Finally, a thin passivation layer of SiO_2 (5 nm) is deposited over the entire membrane surface via atomic layer deposition. A passivation layer is commonly used in nanopore devices integrated with on-chip electrodes to reduce electrochemical reactions between the electrodes and the electrolyte solution [35]. A more detailed description of the fabrication process is given in S1.1 in the Electronic Supplementary Material (ESM). To enable control of the voltage applied to the on-chip electrodes and the electrolyte solution in contact with the membrane we designed a fluidic cell. This fluidic cell consists of a printed circuit board (PCB) to which the on-chip electrodes are wire-bonded. The PCB is then sandwiched between two PTFE blocks containing perfluoroelastomer O-rings to enable fluidic isolation of the electrolyte solution (described more detail in S1.2 in the ESM).

Given the asymmetry of our device geometry, the conduction and breakdown characteristics depend on the direction of the applied electric field [51]. This is because, during a typical CBD experiment (i.e., where the voltage is applied via electrolyte solutions on both sides of the membrane), conduction is limited by oxidation reactions that must occur at the membrane–electrolyte interface [51]. For our asymmetric device geometry, when a negative voltage is applied to the on-chip electrode, an oxidation reaction does not need to occur since electrons are supplied by the metal. This results in an increased conduction across the membrane and breakdown at a lower voltage. In our previous work, we referred to this as the forward-biased configuration. In contrast, when a positive voltage is applied to the on-chip electrodes, an oxidation reaction must occur at the membrane–electrolyte interface (a reduction reaction does not need to occur). This results in a decreased conduction and breakdown at a higher voltage. We referred to this as the reverse-biased configuration in our previous work. Note that a similar mechanism will also likely exist when breakdown is performed by applying a voltage between a conductive atomic force microscope tip and an electrolyte solution in contact with the other side of the membrane as done in previous studies [42].

Unless noted otherwise, CBD was performed using the forward-biased configuration in this work. In particular, an increasingly negative voltage was applied to one of the on-chip electrodes while the electrolyte solution and the other on-chip electrodes were held at 0 V. Figure 1(c) shows CBD measurements performed on four different electrodes on the same membrane. Given that breakdown occurs at a relatively low voltage in the forward-biased configuration (5–6 V for our device geometry), we found that it is necessary to slowly decrease the voltage following breakdown to avoid soft-breakdown events. This is where breakdown occurs but the membrane material is not fully removed to create a nanopore [38]. The voltage protocol used is shown in Fig. 1(c) while a detailed description of the voltage protocol is provided in S1.3 in the ESM. As shown in Fig. 1(c), the leakage current prior to breakdown, and the breakdown voltage is relatively similar for each measurement. This highlights the ability to independently fabricate multiple nanopores in the membrane using our CBD protocol. It is noted that, as shown in S1.4 in the ESM, we are also able to independently fabricate multiple nanopores in the membrane when breakdown is performed in the reverse-biased configuration. However, due to the different conduction and breakdown characteristics depending on the electric field direction, changes in the voltage protocol required to fabricate a single nanopore were required (see S1.3 in the ESM for a description of the voltage protocols).

To confirm the independent fabrication of multiple nanopores using this CBD strategy, we have performed fluorescence imaging of the pores. This technique relies on adding Ca^{2+} ions to the solution on one side of the membrane and the Ca^{2+} indicator Fluo-4 to the solution on the other side of the membrane [41, 52, 53]. When an appropriate voltage is applied across the membrane, Ca^{2+} ions are driven through the nanopore resulting in a fluorescence signal at the nanopore. A detailed description of the procedure used for fluorescence imaging of the nanopores is provided in S1.5 in the ESM. Figure 1(d) shows fluorescence micrographs of the nanopores created by the CBD measurements shown in Fig. 1(c). The images represent a time-series of data with a frame before, during, and after the application of a voltage that drives Ca^{2+} ions through the nanopore. The white dashed box represents the suspended region of SiN_x. The solid red and white lines show the position of the electrodes that CBD was and was not performed on, respectively. There was a fluorescence signal observed in each electrode on which CBD was performed. Differences in the fluorescence intensity of each pore correspond to variations in the pore diameters which is discussed in more detail below. Conversely no fluorescence signal was observed in electrodes on which CBD was not performed. This result confirms the ability to independently localise and fabricate multiple nanopores in the membrane using this CBD strategy. Note, it has previously been shown that CBD can be used to create nanopores that extend through a gold layer on a dielectric membrane [54]. However, it is not trivial that breakdown will also create a nanopore through the passivation layer that was deposited over the electrodes in this work. The above fluorescence images indicate that the nanopore is created through the entire membrane since a large fluorescence signal will only be observed if the Ca^{2+} binds to the indicator dye. We have also performed TEM characterisation of the fabricated nanopores (S1.6 in the ESM). Consistent with previous studies, we observe that the metal is locally removed from a nanoscale region around the fabricated nanopore [54]. While the mechanism of the metal removal is not fully understood, this may result from electrochemical etching of the metal at the high voltages that are applied during breakdown. Future studies characterising how this region of etched metal is affected by the voltage protocol used (e.g., forward vs. reverse-biased) would be of interest.

To obtain statistics of the diameter of the created pores, we have created a single nanopore in the membrane for six different devices using our CBD strategy. After breakdown, reservoirs on both sides of the membrane are filled with a 3.6 M LiCl (10 mM Tris and 0.1mM EDTA at pH 8) buffer solution and the device left for 1 h to stabilise. Following this the ionic current through the nanopore was measured to estimate the pore diameter. The CBD traces and the estimated resulting nanopore diameter are shown in Fig. 2(a). The average diameter of the created pores was 4.1 ± 3.0 nm. One of the devices underwent soft-breakdown where an appreciable ionic current through the pore could not be measured following CBD.

In a typical CBD protocol where breakdown is performed by applying a voltage via electrolyte solutions in contact with both sides of the membrane, the nanopore diameter can be precisely controlled by applying voltage pulses following breakdown and estimating the pore size by measuring the conduction at a low voltage (~ 200 mV) between each pulse [38, 40, 55]. In our CBD strategy a current can be measured between the Ag/AgCl electrode and the small area of the on-chip electrode that is exposed to the solution after breakdown. However, this current can not easily be used to directly estimate the nanopore size [56] since there is a non-negligible resistance associated with charge transfer to the on-chip electrode. However, we have observed that the current measured while reducing the voltage to zero following breakdown
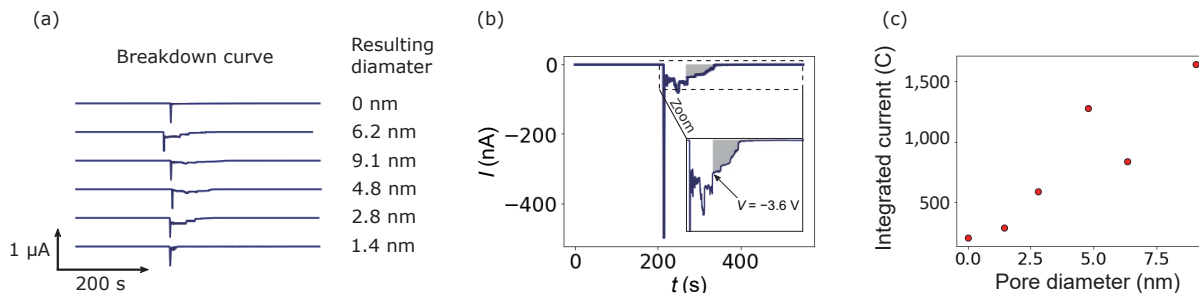
Figure 2 (a) CBD traces for six different chips and the resulting nanopore diameters. For each chip, CBD was performed on a single electrode on the membrane and the resulting pore diameter estimated based on the ionic current through the pore after filling reservoirs on both sides of the membrane with electrolyte solution. (b) An example of CBD trace. The grey region shows the area that was integrated to quantify the current passed after breakdown. The inset shows a zoom of the main figure following breakdown. (c) The current passed after breakdown (quantified as shown in (b)) as a function of the estimated pore diameter following CBD.

correlates to the final nanopore size. In particular, measuring a larger current while reducing the voltage following breakdown generally indicates the formation of a larger nanopore. This can be seen in Fig. 2(a) when comparing the breakdown traces that created a 0 nm pore (i.e., underwent soft breakdown) and the 6.2 nm pore. To quantify the current measured while reducing the voltage following breakdown, we have integrated the current while reducing the voltage from −3.6 to 0 V (grey region in Fig. 2(b)). Integrating the current in this voltage range was found to give the best correlation with the resulting nanopore size. As shown in Fig. 2(c), we observe an increase in the resulting nanopore diameter with increasing current measured following breakdown. This result indicates that precise control over the nanopore size may be possible by using feedback conditions where the voltage is reduced at a rate depending on the measured current for our CBD strategy.

3 Self-aligning nanopores with an on-chip metal nanoconstriction

Above we demonstrated that performing CBD by applying the breakdown voltage between an on-chip electrode and an electrolyte solution in contact with the other side of the membrane enables the independent fabrication of multiple nanopores. To fully exploit this result, it is necessary to utilise alternative sensing mechanisms to ionic current based detection that do not require individual nanopores to be fluidically isolated for their signal to be read out independently. Such alternative readout mechanisms often rely on integrating on-chip nanostructures such as field-effect sensors [18–22], tunnelling nanogaps [23–26], plasmonic nanostructures [57, 58], and radiofrequency antennas [59] with a nanopore. To address this, we extended our CBD strategy to fabricate nanopores that are self-aligned with on-chip nanoelectrodes. In particular, we show that by locally heating the membrane by applying appropriate voltages to the on-chip electrodes we are able to create nanopores self-aligned with complementary nanoelectrodes.

To first understand how heating the membrane affects the breakdown voltage, we have performed CBD under a range of different temperatures. This was done by placing the fluidic cell on a heater plate for 30 min for the temperature of the cell to reach equilibrium. The electrolyte reservoirs were covered during this period to avoid evaporation of the solution. To begin with, these measurements were performed in the typical CBD configuration with electrolyte solution on both sides of the membrane (Fig. 3(a)). We observe a decrease in the breakdown voltage with increasing temperature that is consistent with previous studies [60]. The gradient of the line of best fit (black dashed line) is −109 ± 16 mV/°C. We have also performed similar measurements when the voltage is applied between an on-chip electrode and an electrolyte solution in contact with the other side of the membrane

for the forward-biased (Fig. 3(b)) and reverse-biased (Fig. 3(c)) configurations. For these experiments we observe a similar decrease in the breakdown voltage with increasing temperature. However, it is noted that the gradient of the decrease changes which may be due to the different breakdown voltages and/or conduction mechanism between the two electric field directions. The mechanism for the decrease in breakdown voltage with increasing temperature is not fully understood. This may be a result of increased electron transfer processes at the membrane–electrolyte interface or increased electron transport across the dielectric. Moreover, changes in the conductivity of the electrolyte solution may also contribute to the decrease in the breakdown voltage with increasing temperature. Understanding the exact mechanism of the decrease in breakdown voltage with increasing temperature is outside the scope of this work. Nonetheless, these results indicated that it should be possible to confine nanopore formation to a specific region by locally heating the membrane.

To test if it is possible to confine nanopore formation to a specific region by locally heating the membrane, we fabricated metal nanoconstrictions on SiN$_x$ membranes. We choose to use this device geometry since passing a current through a metal nanoconstriction results in localised Joule heating at the center of the constriction as the current density is highest here. A schematic of this device geometry and experimental setup is shown in Fig. 4(a). False-colour SEM images of the electrodes over the suspended region of SiN$_x$ are shown in Fig. 4(b) . Aside from the different electrode geometry, the device structure is similar to that shown in Fig. 1(a) with the exception of the electrode material (5 nm Cr/30 nm Au) and the passivation layer (5 nm HfO$_2$). A detailed description of the device geometry and the fabrication procedure for these devices are provided in S1.1 in the ESM.

Previous studies have extensively utilised metal nanoconstrictions to create nanogap electrodes via electromigration by passing a large current density through the constriction [26, 61, 62]. Electromigration is a process whereby energy from electrons is transferred to the metal atoms resulting in their migration and the formation of a nanogap [63]. This process is aided by Joule heating at the center of the constriction which increases the mobility of the metal atoms in this region [64]. Indeed, previous studies have demonstrated that the temperature at the center of a gold constriction can reach up to ~ 390 °C prior to electromigration [64] (the exact value will likely vary depending on the geometry of the electrodes). To understand the operating limits of our devices, we increased the voltage applied across the nanoconstriction until a drop in the current was observed indicating the formation of a nanogap via electromigration (S1.7 in the ESM). This typically occurs at voltage of ~ 1.5 V and a corresponding current of ~ 3 mA for our device geometry. Assuming a width of the constriction of 200 nm and a thickness of
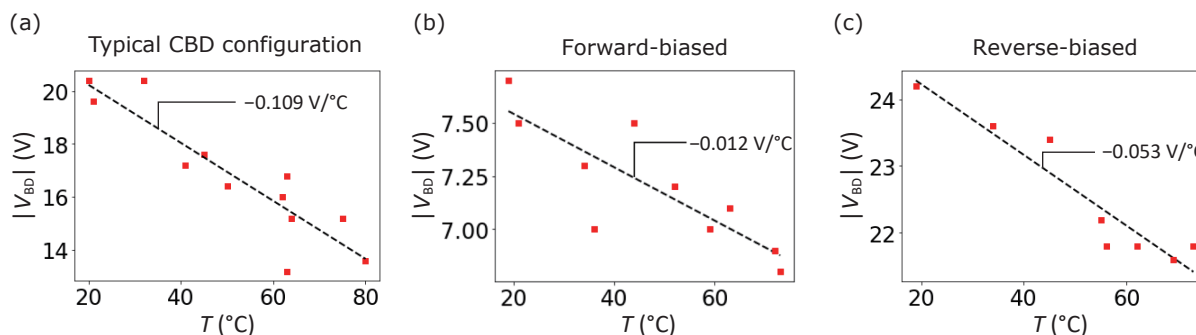
Figure 3 (a) Breakdown voltage as a function of temperature. This is shown for (a) a standard CBD configuration where the voltage is applied via electrolyte solutions in contact with both sides of the membrane. When the voltage is applied between an on-chip electrode and the electrolyte solution in contact with the other side of the membrane in the (b) forward-biased and (c) reverse-biased configurations.
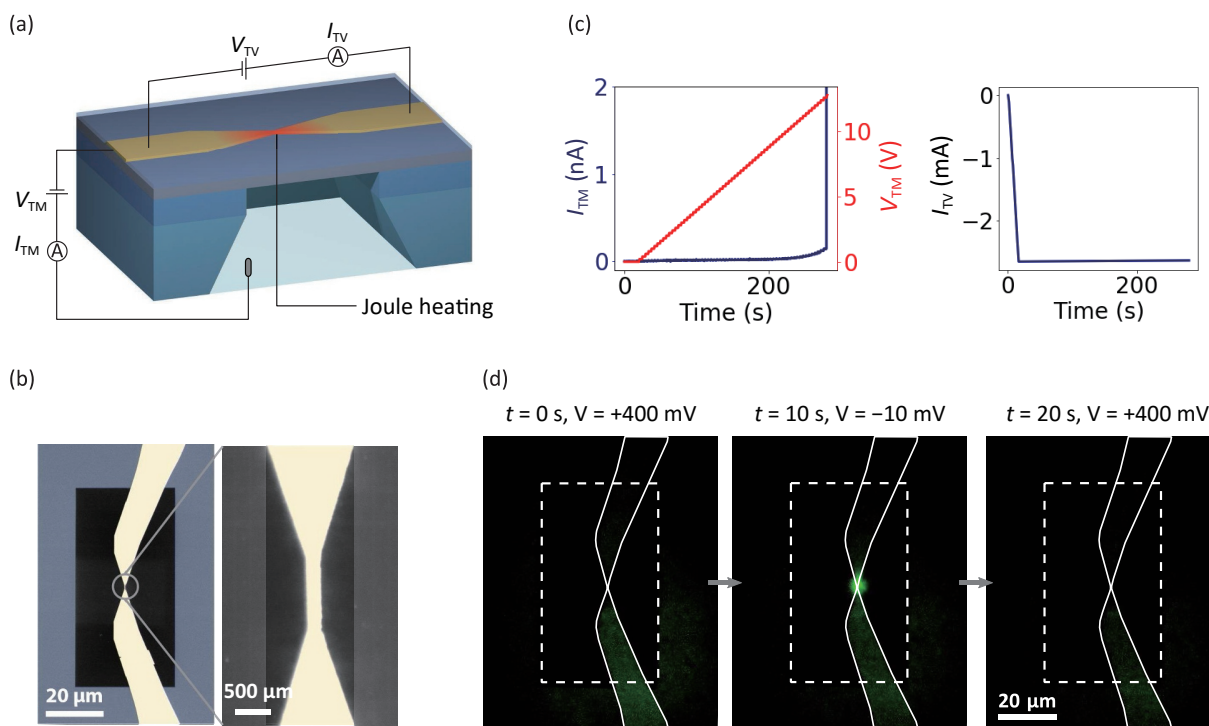

Figure 4 (a) Schematic of the device geometry and the experimental setup used to fabricate nanopores self-aligned with an on-chip metal nanoconstriction. (b) False-colour scanning electron micrographs of the electrode geometry. The left micrograph shows the electrode geometry over the suspended region of SiN_x while the right micrograph shows a higher magnification micrograph at the centre of the metal nanoconstriction. (c) Example traces of the transverse current measured across the metal nanoconstriction (I_{TV}) and the transmembrane current measured across the membrane (I_{TM}) during CBD. The maximum voltage applied across the metal nanoconstriction (V_{TV}) is 1.2 V. (d) Fluorescence images of the nanopore position after CBD. The three micrographs represent an image before (left), during (middle), and after (right) the application of a voltage that drives Ca^{2+} ions through the nanopore. The dashed white box shows the region of suspended SiN_x while the solid white lines show the position of the on-chip electrodes.

30 nm, the current density at the narrowest part of the constriction immediately prior to electromigration is approximately 5×10^{11} A/m².

To perform CBD on these devices, a transverse voltage (V_{TV}) was applied across the metal nanoconstriction while measuring the resulting current (I_{TV}). V_{TV} was limited to 1.2 V to ensure significant Joule heating while avoiding electromigration of the nanoconstriction. Simultaneous to this, an increasing transmembrane voltage (V_{TM}) was applied between the metal nanoconstriction and the electrolyte solution while measuring the resulting current (I_{TM}). When a spike in I_{TM} was observed indicating nanopore formation both V_{TM} and V_{TV} were immediately reduced to zero (we did not observe any issues with soft-breakdown when immediately reducing the voltage for this device geometry). Figure 4(c) shows typical CBD measurements while simultaneously heating the membrane by passing a large current density through the metal nanoconstriction. To determine the position of the resulting nanopore, fluorescence imaging was

performed. As shown in Fig. 4(d), the nanopore formed at the narrowest part of the constriction. This is consistent with the fact that the Joule heating is highest in this region. This result was reproducible across multiple devices (S1.8 in the ESM). We have also performed SEM imagings of the devices following breakdown (S1.9 in the ESM). These images indicate that the pore formed at the narrowest part of the nanoconstriction (the narrowest part of the constriction is 500 nm long) indicating that nanoscale alignment is indeed possible using this method.

It is noted that following breakdown, the current measured across the metal nanoconstriction dropped to approximately zero (Fig. 4(c)). This suggests that damage has occurred to the metal nanoconstriction during breakdown such that the two sides of the constriction are no longer electrically connected. This was confirmed from SEM images of the device after nanopore formation (S1.9 in the ESM). Such damage may be due to the significant heating which increases the conductivity of the electrolyte leading to rapid nanopore expansion following

breakdown [40]. Indeed, nanopores created using the above protocol were typically larger than ~ 50 nm as observed from SEM images and confirmed by measuring the ionic current through the pore following breakdown. Due to limits in the electronics used in this work, a relatively slow feedback frequency was used to reduce the voltage after breakdown (the voltage is reduced up to ~ 70 ms following breakdown). It is likely that employing faster feedback conditions will enable the creation of smaller nanopores with minimal damage to the surrounding nanoelectrodes. Changing the device geometry such as (i) reducing the thicknesses of the SiN$_x$ membrane, (ii) modifying the electrode geometry or material, and (iii) changing the thickness or composition of the passivation layer may also enable the fabrication of smaller nanopores. This is an area that should be explored further in future studies.

4 Biomolecular sensing

To demonstrate the utility of the nanopores created using the CBD strategy introduced here, we have performed biomolecular sensing using these devices. To do this, a single nanopore was created using the CBD protocol described in Sec. 2. Following breakdown, reservoirs on both sides of the membrane were filled with 3.6 M LiCl, 10 mM Tris, and 0.1 mM EDTA at pH 8 solution and the device was left overnight for the ionic current through the nanopore to stabilise [50, 65]. Following this, a linear ionic current as a function of the applied voltage was measured (S1.10 in the ESM). The size of the nanopore estimated from the conductance is ~ 13 nm [56]. The noise spectrum of the ionic current of the created pores is comparable to that observed in solid-state nanopores created via TEM drilling [66] or CBD when the breakdown voltage is applied via electrolyte solutions in contact with both sides of the membrane [38] (S1.10 in the ESM).

To demonstrate the ability to perform single-molecule biosensing using these nanopores, 1 kbp dsDNA (NoLimits DNA, ThermoFisher) was added to the *cis* chamber resulting in a DNA concentration of ~ 5 nM in that reservoir. Figure 5(a)(i) shows representative current-time traces demonstrating DNA translocation events through the created nanopore at various applied voltages. The peak current blockage and dwell time of the extracted translocation events are also shown in scatter plots (Fig. 5(a)(ii)) and violin plots (Fig. 5(a)(iii)). Closer inspection of the extracted peak current blockade, as well as direct visualisation of the translocation events (Fig. 5(b)) reveals the presence of single-level and two-level blockade events. This is typical of DNA
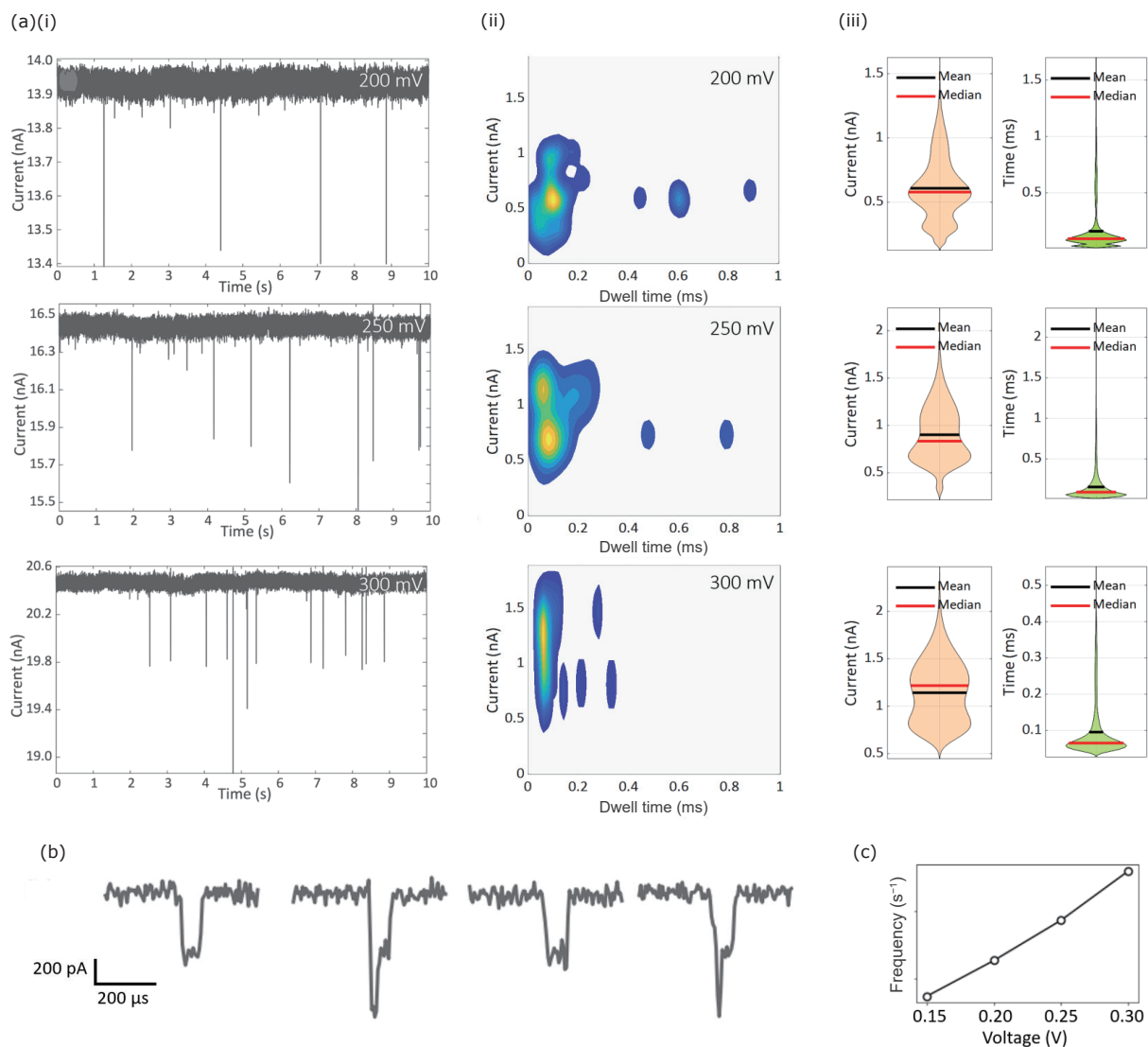

Figure 5 (a) Representative current-time traces demonstrating translocation of 1 kbp dsDNA in 3.6 M LiCl through a nanopore created via the procedure described in Sec. 2. (i) For visualisation the traces were processed using a 10 kHz digital Bessel filter. (ii) Scatter plots (peak event current vs. dwell time) and (iii) violin plots for DNA translocation events at 200, 250, and 300 mV. (b) Examples of individually events demonstrating the translocation of folded and unfolded DNA. (c) Translocation frequency as a function of the applied voltage. All experiments were performed by applying the voltage to the Ag/AgCl electrode in the *trans* chamber while holding the Ag/AgCl in the *cis* chamber and the on-chip electrodes at ground.

translocation through solid-state pores with a diameter twice larger than the diameter of a dsDNA molecule (~ 2.3 nm) [67]. The two-level current blockades correspond to the translocation of DNA in a folded manner through the nanopore while the single-level current blockades correspond to the translocation of DNA in an unfolded manner [67]. A linear increase in the translocation frequency as a function of applied voltage is also observed (Fig. 5(c)). This indicates that the translocation frequency is primarily limited by diffusion of the analyte to the capture radius of the pore as expected for our nanopore geometry [67, 68]. These results confirm that nanopores fabricated via the CBD strategy introduced here can be used for single-molecule biosensing applications.

5 Conclusion and outlook

Here we have introduced a new CBD strategy to fabricate solid-state nanopores whereby breakdown is performed by applying a voltage between an on-chip electrode and an electrolyte solution in contact with the other side of the membrane. Since the applied electric field is localised to the on-chip electrode, this technique enables us to independently fabricate and localise multiple nanopores in the membrane. Moreover, by using the on-chip electrodes to locally heat the membrane we are able to create nanopores that are self-aligned with on-chip nanostructures. This was demonstrated by performing CBD simultaneous to pass a large current density through a metal nanoconstriction to induce localised Joule heating. Here, it was shown that the fabricated nanopore forms at the narrowest part of the constriction where Joule heating is highest. We believe this is a versatile technique that could be used to integrate nanopores with a range of on-chip nanostructures such as field-effect sensors and nanogap electrodes. In S1.11 in the ESM we describe some possible geometries and voltage protocols that could be explored in future studies to self-align nanopores with various on-chip nanostructures via this technique.

It is noted that the CBD strategy presented here is similar to tip controlled localised breakdown (TCLB), where breakdown is performed by applying a voltage between a conductive atomic force microscope (AFM) tip and an electrolyte solution in contact with the other side of the membrane. However, our strategy possesses advantages over this method for the case where a nanopore is to be integrated with an on-chip electrode in the final device geometry. Given electrodes are already on the membrane surface for such device geometries, our technique requires no additional equipment or fabrication steps. This simplifies our technique compared to TCLB which requires an AFM to perform breakdown. Moreover, since the nanopore is self-aligned with the on-chip electrode, our technique should be faster than TCLB which requires AFM imaging of the local region to align nanopores with additional structures. On the other hand, for applications that require an array of nanopores but no on-chip electrodes (e.g., for optical nanopore sensing applications) TCLB may be the preferable method. This is because, the CBD strategy presented here would require the deposition of electrodes on the membrane thus complicating the fabrication procedure. We therefore believe that the nanopore fabrication strategy developed here adds to the growing suite of CBD methods with the preferable technique depending on the final application.

CBD is quickly becoming one of the most popular techniques to fabricate solid-state nanopores. This technique is particularly appealing as it does not require expensive equipment and can be fully automated thus making it accessible to the wider research community. Furthermore, CBD creates nanopores in the electrolyte environment which measurements are performed in.

This can reduce problems associated with wetting of the nanopore. Our new CBD strategy extends this popular nanopore fabrication technique for applications where it is desirable to fabricate arrays of nanopores integrated with on-chip nanostructures. While our work demonstrates the feasibility of this approach, there is still a significant amount of work that needs to be done before this CBD strategy reaches its full potential. In particular, future work should concentrate on better characterising the size distribution of the fabricated nanopores. The development of active voltage control based on the measured current after breakdown will also be useful in better controlling the size distribution of the created pores. Another area of interest would be to characterise the pore density obtainable using this strategy. This will be limited by the area of electrolyte that comes into contact with the front side of the membrane following breakdown. It may be possible to characterise this (down to the diffraction limit) by performing our CBD strategy *in situ* in a light microscope. Lastly, further research should be performed to minimise damage to the on-chip electrodes during breakdown. This should be possible by utilising faster feedback conditions as well as modifying the device geometry (e.g., using a thinner membrane). With this further development, we believe that our CBD strategy can significantly accelerate research into the development of solid-state nanopores integrated with complementary nanostructures and open up routes for the commercial development of these devices.

Electronic Supplementary Material: Supplementary material (fabrication/experimental procedure, TEM images, SEM images, and potential future works) is available in the online version of this article at https://doi.org/10.1007/s12274-022-4535-8.

References

[1] Yusko, E. C.; Bruhn, B. R.; Eggenberger, O. M.; Houghtaling, J.; Rollings, R. C.; Walsh, N. C.; Nandivada, S.; Pindrus, M.; Hall, A. R.; Sept, D. et al. Real-time shape approximation and fingerprinting of single proteins using a nanopore. *Nat. Nanotechnol.* **2017**, *12*, 360–367.

[2] Alfaro, J. A.; Bohländer, P.; Dai, M. J.; Filius, M.; Howard, C. J.; Van Kooten, X. F.; Ohayon, S.; Pomorski, A.; Schmid, S.; Aksimentiev, A. et al. The emerging landscape of single-molecule protein sequencing technologies. *Nat. Methods* **2021**, *18*, 604–617.

[3] Restrepo-Pérez, L.; Joo, C.; Dekker, C. Paving the way to single-molecule protein sequencing. *Nat. Nanotechnol.* **2018**, *13*, 786–796.

[4] Bell, N. A. W.; Keyser, U. F. Digitally encoded DNA nanostructures for multiplexed, single-molecule protein sensing with nanopores. *Nat. Nanotechnol.* **2016**, *11*, 645–651.

[5] Chen, K. K.; Zhu, J. B.; Bošković, F.; Keyser, U. F. Nanopore-based DNA hard drives for rewritable and secure data storage. *Nano Lett.* **2020**, *20*, 3754–3760.

[6] Chuah, K.; Wu, Y. F.; Vivekchand, S. R. C.; Gaus, K.; Reece, P. J.; Micolich, A. P.; Gooding, J. J. Nanopore blockade sensors for ultrasensitive detection of proteins in complex biological samples. *Nat. Commun.* **2019**, *10*, 2109.

[7] Wu, Y. F.; Yao, Y.; Cheong, S.; Tilley, R. D.; Gooding, J. J. Selectively detecting attomolar concentrations of proteins using gold lined nanopores in a nanopore blockade sensor. *Chem. Sci.* **2020**, *11*, 12570–12579.

[8] Cai, S. L.; Pataillot-Meakin, T.; Shibakawa, A.; Ren, R.; Bevan, C. L.; Ladame, S.; Ivanov, A. P.; Edel, J. B. Single-molecule amplification-free multiplexed detection of circulating microRNA cancer biomarkers from serum. *Nat. Commun.* **2021**, *12*, 3515.

[9] Rozevsky, Y.; Gilboa, T.; Van Kooten, X. F.; Kobelt, D.; Huttner, D.; Stein, U.; Meller, A. Quantification of mRNA expression using single-molecule nanopore sensing. *ACS Nano* **2020**, *14*, 13964–13974.

[10] Dekker, C. Solid-state nanopores. *Nat. Nanotechnol.* **2007**, *2*, 209–215.

[11] Miles, B. N.; Ivanov, A. P.; Wilson, K. A.; Doğan, F.; Japrung, D.; Edel, J. B. Single molecule sensing with solid-state nanopores: Novel materials, methods, and applications. *Chem. Soc. Rev.* **2013**, *42*, 15–28.

[12] Xue, L.; Yamazaki, H.; Ren, R.; Wanunu, M.; Ivanov, A. P.; Edel, J. B. Solid-state nanopore sensors. *Nat. Rev. Mater.* **2020**, *5*, 952.

[13] Tsutsui, M.; Ryuzaki, S.; Yokota, K.; He, Y. H.; Washio, T.; Tamada, K.; Kawai, T. Field effect control of translocation dynamics in surround-gate nanopores. *Commun. Mater.* **2021**, *2*, 29.

[14] Luan, B. Q.; Peng, H. B.; Polonsky, S.; Rossnagel, S.; Stolovitzky, G.; Martyna, G. Base-by-base ratcheting of single stranded DNA through a solid-state nanopore. *Phys. Rev. Lett.* **2010**, *104*, 238103.

[15] Paik, K. H.; Liu, Y.; Tabard-Cossa, V.; Waugh, M. J.; Huber, D. E.; Provine, J.; Howe, R. T.; Dutton, R. W.; Davis, R. W. Control of DNA capture by nanofluidic transistors. *ACS Nano* **2012**, *6*, 6767–6775.

[16] Nam, S. W.; Rooks, M. J.; Kim, K. B.; Rossnagel, S. M. Ionic field effect transistors with sub-10 nm multiple nanopores. *Nano Lett.* **2009**, *9*, 2044–2048.

[17] Freedman, K. J.; Otto, L. M.; Ivanov, A. P.; Barik, A.; Oh, S. H.; Edel, J. B. Nanopore sensing at ultra-low concentrations using single-molecule dielectrophoretic trapping. *Nat. Commun.* **2016**, *7*, 10217.

[18] Xie, P.; Xiong, Q. H.; Fang, Y.; Qing, Q.; Lieber, C. M. Local electrical potential detection of DNA by nanowire-nanopore sensors. *Nat. Nanotechnol.* **2012**, *7*, 119–125.

[19] Traversi, F.; Raillon, C.; Benameur, S. M.; Liu, K.; Khlybov, S.; Tosun, M.; Krasnozhon, D.; Kis, A.; Radenovic, A. Detecting the translocation of DNA through a nanopore using graphene nanoribbons. *Nat. Nanotechnol.* **2013**, *8*, 939–945.

[20] Heerema, S. J.; Vicarelli, L.; Pud, S.; Schouten, R. N.; Zandbergen, H. W.; Dekker, C. Probing DNA translocations with inplane current signals in a graphene nanoribbon with a nanopore. *ACS Nano* **2018**, *12*, 2623–2633.

[21] Graf, M.; Lihter, M.; Altus, D.; Marion, S.; Radenovic, A. Transverse detection of DNA using a MoS_2 nanopore. *Nano Lett.* **2019**, *19*, 9075–9083.

[22] Zhu, X.; Li, X. J.; Gu, C. M.; Ye, Z.; Cao, Z.; Zhang, X. Y.; Jin, C. H.; Liu, Y. Monolithic integration of vertical thin-film transistors in nanopores for charge sensing of single biomolecules. *ACS Nano* **2021**, *15*, 9882–9889.

[23] Ivanov, A. P.; Instuli, E.; McGilvery, C. M.; Baldwin, G.; McComb, D. W.; Albrecht, T.; Edel, J. B. DNA tunneling detector embedded in a nanopore. *Nano Lett.* **2011**, *11*, 279–285.

[24] Ivanov, A. P.; Freedman, K. J.; Kim, M. J.; Albrecht, T.; Edel, J. B. High precision fabrication and positioning of nanoelectrodes in a nanopore. *ACS Nano* **2014**, *8*, 1940–1948.

[25] Fanget, A.; Traversi, F.; Khlybov, S.; Granjon, P.; Magrez, A.; Forró, L.; Radenovic, A. Nanopore integrated nanogaps for DNA detection. *Nano Lett.* **2014**, *14*, 244–249.

[26] Tsutsui, M.; Rahong, S.; Iizumi, Y.; Okazaki, T.; Taniguchi, M.; Kawai, T. Single-molecule sensing electrode embedded in-plane nanopore. *Sci. Rep.* **2011**, *1*, 46.

[27] Tang, L. H.; Nadappuram, B. P.; Cadinu, P.; Zhao, Z. Y.; Xue, L.; Yi, L.; Ren, R.; Wang, J. W.; Ivanov, A. P.; Edel, J. B. Combined quantum tunnelling and dielectrophoretic trapping for molecular analysis at ultra-low analyte concentrations. *Nat. Commun.* **2021**, *12*, 913.

[28] Cecchini, M. P.; Wiener, A.; Turek, V. A.; Chon, H.; Lee, S.; Ivanov, A. P.; McComb, D. W.; Choo, J.; Albrecht, T.; Maier, S. A. et al. Rapid ultrasensitive single particle surface-enhanced Raman spectroscopy using metallic nanopores. *Nano Lett.* **2013**, *13*, 4602–4609.

[29] Freedman, K. J.; Crick, C. R.; Albella, P.; Barik, A.; Ivanov, A. P.; Maier, S. A.; Oh, S. H.; Edel, J. B. On-demand surface- and tip-enhanced Raman spectroscopy using dielectrophoretic trapping and nanopore sensing. *ACS Photonics* **2016**, *3*, 1036–1044.

[30] Shi, X.; Gao, R.; Ying, Y. L.; Si, W.; Chen, Y. F.; Long, Y. T. A scattering nanopore for single nanoentity sensing. *ACS Sens.* **2016**, *1*, 1086–1090.

[31] Verschueren, D. V.; Pud, S.; Shi, X.; de Angelis, L.; Kuipers, L.; Dekker, C. Label-free optical detection of DNA translocations through plasmonic nanopores. *ACS Nano* **2019**, *13*, 61–70.

[32] Shi, X.; Verschueren, D. V.; Dekker, C. Active delivery of single DNA molecules into a plasmonic nanopore for label-free optical sensing. *Nano Lett.* **2018**, *18*, 8003–8010.

[33] Chang, S.; He, J.; Kibel, A.; Lee, M.; Sankey, O.; Zhang, P. M.; Lindsay S. Tunnelling readout of hydrogen-bonding-based recognition. *Nat. Nanotechnol.* **2009**, *4*, 297–301.

[34] Parkin, W. M.; Drndić, M. Signal and noise in FET-nanopore devices. *ACS Sens.* **2018**, *3*, 313–319.

[35] Healy, K.; Ray, V.; Willis, L. J.; Peterman, N.; Bartel, J.; Drndić, M. Fabrication and characterization of nanopores with insulated transverse nanoelectrodes for DNA sensing in salt solution. *Electrophoresis* **2012**, *33*, 3488–3496.

[36] Fried, J. P.; Swett, J. L.; Bian, X. Y.; Mol, J. A. Challenges in fabricating graphene nanodevices for electronic DNA sequencing. *MRS Commun.* **2018**, *8*, 703–711.

[37] Kwok, H.; Briggs, K.; Tabard-Cossa, V. Nanopore fabrication by controlled dielectric breakdown. *PLoS One* **2014**, *9*, e92880.

[38] Waugh, M.; Briggs, K.; Gunn, D.; Gibeault, M.; King, S.; Ingram, Q.; Jimenez, A. M.; Berryman, S.; Lomovtsev, D.; Andrzejewski, L. et al. Solid-state nanopore fabrication by automated controlled breakdown. *Nat. Protoc.* **2020**, *15*, 122–143.

[39] Fried, J. P.; Swett J. L.; Nadappuram, B. P.; Mol, J. A.; Edel, J. B.; Ivanov, A. P.; Yates, J. R. *In situ* solid-state nanopore fabrication. *Chem. Soc. Rev.* **2021**, *50*, 4974–4992.

[40] Leung, C.; Briggs, K.; Laberge, M. P.; Peng, S.; Waugh, M.; V. Tabard-Cossa. Mechanisms of solid-state nanopore enlargement under electrical stress. *Nanotechnology* **2020**, *31*, 44LT01.

[41] Zrehen, A.; Gilboa, T.; Meller, A. Real-time visualization and sub-diffraction limit localization of nanometer-scale pore formation by dielectric breakdown. *Nanoscale* **2017**, *9*, 16437–16445.

[42] Zhang, Y. N.; Miyahara, Y.; Derriche, N.; Yang, W.; Yazda, K.; Capaldi, X.; Liu, Z. Z.; Grutter, P.; Reisner, W. Nanopore formation via Tip-controlled local breakdown using an atomic force microscope. *Small Methods* **2019**, *3*, 1900147.

[43] Yazda, K.; Bleau, K.; Zhang, Y. N.; Capaldi, X.; St-Denis, T.; Grutter, P.; Reisner, W. W. High osmotic power generation via nanopore arrays in hybrid hexagonal boron nitride/silicon nitride membranes. *Nano Lett.* **2021**, *21*, 4152–4159.

[44] Carlsen, A. T.; Briggs, K.; Hall, A. R.; Tabard-Cossa, V. Solid-state nanopore localization by controlled breakdown of selectively thinned membranes. *Nanotechnology* **2017**, *28*, 085304.

[45] Arcadia, C. E.; Reyes, C. C.; Rosenstein, J. K. *In situ* nanopore fabrication and single-molecule sensing with microscale liquid contacts. *ACS Nano* **2017**, *11*, 4907–4915.

[46] Yin, B. H.; Fang, S. X.; Zhou, D. M.; Liang, L. Y.; Wang, L.; Wang, Z. B.; Wang, D. Q.; Yuan, J. H. Nanopore fabrication via transient high electric field controlled breakdown and detection of single RNA molecules. *ACS Appl. Bio Mate.* **2020**, *3*, 6368–6375.

[47] Tahvildari, R.; Beamish, E.; Tabard-Cossa, V.; Godin, M. Integrating nanopore sensors within microfluidic channel arrays using controlled breakdown. *Lab Chip* **2015**, *15*, 1407–1411.

[48] Spitzberg, J. D.; van Kooten, X. F.; Bercovici, M.; Meller, A. Microfluidic device for coupling isotachophoretic sample focusing with nanopore single-molecule sensing. *Nanoscale* **2020**, *12*, 17805–17811.

[49] St-Denis, T.; Yazda, K.; Capaldi, X.; Bustamante, J.; Safari, M.; Miyahara, Y.; Zhang, Y.; Grutter, P.; Reisner, W. An apparatus based on an atomic force microscope for implementing tip-controlled local breakdown. *Rev. Sci. Instrum.* **2019**, *90*, 123703.

[50] Pud, S.; Verschueren, D.; Vukovic, N.; Plesa, C.; Jonsson, M. P.; Dekker, C. Self-aligned plasmonic nanopores by optically controlled dielectric breakdown. *Nano Lett.* **2015**, *15*, 7112–7117.

[51] Fried, J. P.; Swett, J. L.; Nadappuram, B. P.; Fedosyuk, A.; Sousa, P. M.; Briggs, D. P.; Ivanov, A. P.; Edel, J. B.; Mol, J. A.; Yates, J. R. Understanding electrical conduction and nanopore formation during controlled breakdown. *Small* **2021**, *17*, 2102543.

[52] Anderson, B. N.; Assad, O. N.; Gilboa, T.; Squires, A. H.; Bar, D.; Meller, A. Probing solid-state nanopores with light for the detection of unlabeled analytes. *ACS Nano* **2014**, *8*, 11836–11845.

[53] Ivankin, A.; Henley, R. Y.; Larkin, J.; Carson, S.; Toscano, M. L.; Wanunu, M. Label-free optical detection of biomolecular translocation through nanopore arrays. *ACS Nano* **2014**, *8*, 10774–10781.

[54] Kwok, H.; Waugh, M.; Bustamante, J.; Briggs, K.; Tabard-Cossa, V. Long passage times of short ssDNA molecules through metallized nanopores fabricated by controlled breakdown. *Adv. Funct. Mater.* **2014**, *24*, 7745–7753.

[55] Beamish, E.; Kwok, H.; Tabard-Cossa, V.; Godin, M. Precise control of the size and noise of solid-state nanopores using high electric fields. *Nanotechnology* **2012**, *23*, 405301.

[56] Kowalczyk, S. W.; Grosberg, A. Y.; Rabin, Y.; Dekker, C. Modeling the conductance and DNA blockade of solid-state nanopores. *Nanotechnology* **2011**, *22*, 315101.

[57] Spitzberg, J. D.; Zrehen, A.; van Kooten, X. F.; Meller, A. Plasmonic-nanopore biosensors for superior single-molecule detection. *Adv. Mater.* **2019**, *31*, 1900422.

[58] Garoli, D.; Yamazaki, H.; Maccaferri, N.; Wanunu, M. Plasmonic nanopores for single-molecule detection and manipulation: Toward sequencing applications. *Nano Lett.* **2019**, *19*, 7553–7562.

[59] Bhat, A.; Gwozdz, P. V.; Seshadri, A.; Hoeft, M.; Blick, R. H. Tank circuit for ultrafast single-particle detection in micropores. *Phys. Rev. Lett.* **2018**, *121*, 078102.

[60] Yanagi, I.; Takeda, K. I. Current-voltage characteristics of SiN membranes in solution. *ACS Appl. Electron. Mater.* **2020**, *2*, 2760–2771.

[61] Gehring, P.; Thijssen, J. M.; van der Zant, H. S. J. Single-molecule quantum-transport phenomena in break junctions. *Nat. Rev. Phys.* **2019**, *1*, 381–396.

[62] Perrin, M. L.; Burzurí, E.; van der Zant, H. S. J. Single-molecule transistors. *Chem. Soc. Rev.* **2015**, *44*, 902–919.

[63] Hadeed, F. O.; Durkan, C. Controlled fabrication of 1−2 nm nanogaps by electromigration in gold and gold-palladium nanowires. *Appl. Phys. Lett.* **2007**, *91*, 123120.

[64] Jeong, W.; Kim, K.; Kim, Y.; Lee, W.; Reddy, P. Characterization of nanoscale temperature fields during electromigration of nanowires. *Sci. Rep.* **2014**, *4*, 5690.

[65] Briggs, K.; Kwok, H.; Tabard-Cossa, V. Automated fabrication of 2-nm solid-state nanopores for nucleic acid analysis. *Small* **2014**, *10*, 2077–2086.

[66] Fragasso, A.; Schmid, S.; Dekker, C. Comparing current noise in biological and solid-state nanopores. *ACS Nano* **2020**, *14*, 1338–1349.

[67] Chen, P.; Gu, J. J.; Brandin, E.; Kim, Y. R.; Wang, Q.; Branton, D. Probing single DNA molecule transport using fabricated nanopores. *Nano Lett.* **2004**, *4*, 2293–2298.

[68] Grosberg, A. Y.; Rabin, Y. DNA capture into a nanopore: Interplay of diffusion and electrohydrodynamics. *J. Chem. Phys.* **2010**, *133*, 165102.